SOILS AND FOUNDATIONS Vol. 44, No. 1, 25–38, Feb. 2004
Japanese Geotechnical Society

THE INFLUENCE OF BUILDING WEIGHT ON TUNNELLING-INDUCED GROUND AND BUILDING DEFORMATION

JAN N. FRANZIUS[i], DAVID M. POTTS[ii], TREVOR I. ADDENBROOKE[iii] and JOHN B. BURLAND[iv]

ABSTRACT

In urban areas, the ground movements induced by tunnelling can distort and damage overlying buildings. Potts and Addenbrooke (1997) presented new design charts to assist in the assessment of building damage in response to tunnelling. The charts were based on the results of two-dimensional plane-strain finite element analyses considering variations in the bending and axial stiffness of a building relative to the soil stiffness, the building's width, its position relative to the tunnel axis, and the tunnel depth. In all cases, weightless elastic beams represented the building. This paper presents the results of analyses that additionally consider building weight in order to investigate its influence on the tunnelling-induced deformation of a structure.

The mechanisms that control this interaction problem are investigated. It is demonstrated how the application of building load changes the stress regime in the ground and how this stress change alters tunnelling induced ground and building deformation.

The results of a parametric study are used to quantify the effect of a building's self weight. This paper shows that the trend in deflection ratio and horizontal strain with building stiffness is very similar for a wide range of loads investigated. Following the approach of Potts and Addenbrooke (1997), the deformation values are then compared with the greenfield cases to give modification factors. The results reveal an increase in these factors with weight. On the other hand, when plotted against relative stiffness the results are shown to be close to the 'weightless' design curves provided by Potts and Addenbrooke (1997).

Key words: differential, finite element method, numerical analysis, tunnel, underground structure (**IGC**: E12/E13/H5)

INTRODUCTION

The prediction of building distortion induced by tunnel construction is now a key issue in the planning process of any new underground project. This soil-structure interaction problem is, however, not well understood. As a result, present techniques for assessing potential building damage due to underground excavations are conservative. It is therefore important not only to refine the design approach but also to obtain a better understanding of the mechanisms which control this interaction problem.

Current design practice is essentially an empirical approach based on settlement data from recent tunnelling projects (O'Reilly and New, 1982). For the prediction of building subsidence the characteristics of the structure are neglected and the expected deformed shape of a greenfield site is applied in order to assess the damage. For this assessment limiting criteria such as deflection ratio DR, defined in Fig. 1, and horizontal strain ε_h (Burland and Wroth, 1974; Boscarding and Cording, 1989) are used. Interaction diagrams, as shown in Fig. 2, then relate these measures to a damage category system in

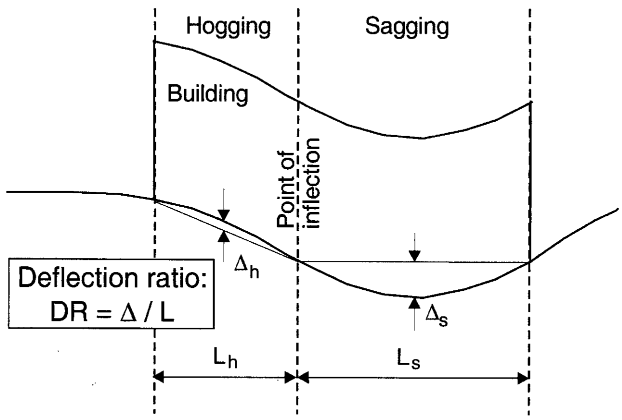

Fig. 1. Building damage parameter: Definition of deflection ratio

[i] Research Student, Department of Civil and Environmental Engineering, Imperial College of Science Technology and Medicine, London SW7 2BU (j.n.franzius@gmx.de).
[ii] Professor, Imperial College, ditto.
[iii] Formerly Lecturer, Imperial College, ditto.
[iv] Professor, Imperial College, ditto.
Manuscript was received for review on November 29, 2002.
Written discussions on this paper should be submitted before September 1, 2004 to the Japanese Geotechnical Society, Sugayama Bldg. 4F, Kanda Awaji-cho 2-23, Chiyoda-ku, Tokyo 101-0063, Japan. Upon request the closing date may be extended one month.

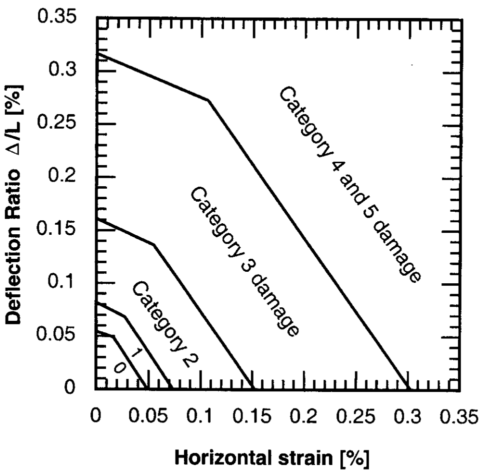

Fig. 2. Relationship of damage category to deflection ratio and horizontal tensile strain for hogging (after Burland, 1995)

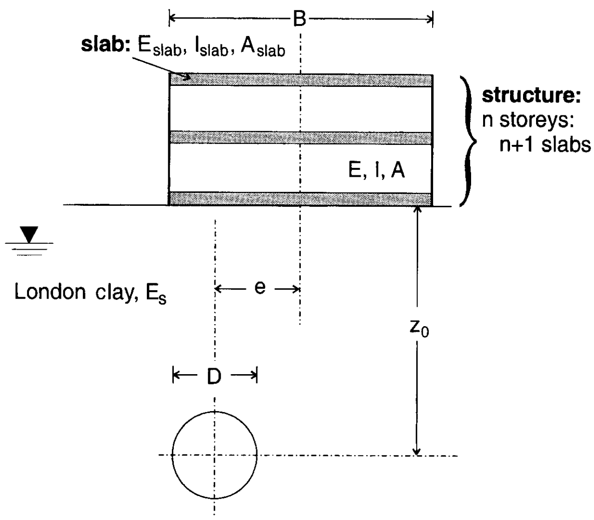

Fig. 3. Geometry of the problem

which aesthetic damage is described by categories 0, 1 and 2 while damage in categories 3 to 5 affect serviceability and structural stability (Burland, 1995). This approach can be conservative as it assumes the building to be infinitely flexible and to follow the greenfield settlement trough.

Potts and Addenbrooke (1997) introduced the possibility of including building stiffness into this design approach. The basis of the new method was an extensive parametric study using two-dimensional (2D) finite element (FE) analyses. By including the structure's stiffness into the design approach it is now possible to predict the critical strain in the building more realistically. A simplification in this work was that the buildings were modelled weightless. This paper explores the influence of building weight on the soil-structure interaction problem.

THE RELATIVE STIFFNESS APPROACH

Potts and Addenbrooke (1997) proposed a method which includes the stiffness of a structure in the prediction of its deformation due to tunnelling induced subsidence. They presented the results of a parametric study including over 100 2D plane strain FE analyses. In their study, the structure was represented by an elastic beam. The beam was considered weightless to enable the authors to investigate the effect of building stiffness uncoupled from other factors. The soil was modelled using non-linear elastic perfectly plastic parameters appropriate to London clay. A wide range of stiffness parameters and geometries were investigated. The stiffness of the building was then related to the stiffness of the soil using relative stiffness parameters which are defined as:

$$\rho^* = \frac{EI}{E_s(B/2)^4} \quad \alpha^* = \frac{EA}{E_s(B/2)} \tag{1}$$

where E is the Young's modulus of the structure; I is its second moment of area and A is its cross sectional area; E_s is the soil's secant stiffness obtained at 0.01% axial strain in a triaxial compression test performed on a sample retrieved from half of the tunnel depth z_0, defined in Fig. 3, (for the soil profile used in their analysis E_s was 103 MPa and 163 MPa for tunnel depths of $z_0 = 20$ m and 34 m respectively) and B is the width of the structure. The relative bending stiffness is given by ρ^*, while α^* is a measure for the relative axial stiffness. In plane strain analysis α^* is dimensionless while ρ^* has the dimension [1/m].

The parameter ρ^* is associated with the deflection ratios DR_{hog} (hogging) and DR_{sag} (sagging) while α^* is associated with the horizontal strain ε_{ht} (tensile) and ε_{hc} (compressive). Potts and Addenbrooke (1997) related these quantities to greenfield conditions using modification factors:

$$M^{DR_{hog}} = \frac{DR_{hog}}{DR^{g}_{hog}} \quad M^{DR_{sag}} = \frac{DR_{sag}}{DR^{g}_{sag}} \tag{2a}$$

for the hogging and sagging deflection ratio DR respectively and:

$$M^{\varepsilon_{ht}} = \frac{\varepsilon_{ht}}{\varepsilon^{g}_{ht}} \quad M^{\varepsilon_{hc}} = \frac{\varepsilon_{hc}}{\varepsilon^{g}_{hc}} \tag{2b}$$

for the tensile and compressive horizontal strain respectively. The index 'g' denotes the corresponding parameter for greenfield conditions. The results of the analyses were presented as plots of modification factor M^{DR} versus relative bending stiffness ρ^* and $M^{\varepsilon h}$ versus α^*. All the results presented by Potts and Addenbrooke (1997) lay within a narrow range in these graphs. Upper bounds were then given to these data to provide a conservative estimate of the variation of the modification factors with respect to the structure's relative stiffness.

These curves (Fig. 4 shows as an example the chart for M^{DR}) are then used for design purposes (Potts and Addenbrooke, 1997): As a first step, the settlement profile for the particular tunnel depth, volume loss etc., is estimated using empirical formulas described by O'Reilly and New (1982). For these greenfield conditions the deflection ratios and horizontal strains are calculated.

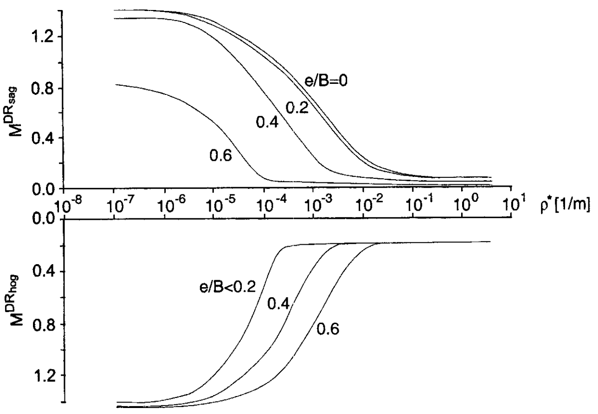

Fig. 4. Design curves for modification factors M^{DR} (after Potts and Addenbrooke, 1997)

The stiffness of the building is then estimated giving the relative stiffness parameters. Finally, the modification factors are found from the design curves. Applying these values to the deflection ratio and strain obtained for greenfield conditions leads to modified values which take account of the building stiffness. With these data the building damage category can be assessed using diagrams as shown in Fig. 2.

FINITE ELEMENT ANALYSIS

To investigate the influence of building load on the deformation behaviour of the ground and building in response to tunnelling, a set of FE analyses were undertaken similar to those performed by Potts and Addenbrooke (1997). This work focuses on the influence of building load, so one building width is considered in combination with two tunnel depths and a wide range of building stiffnesses and loads. The Imperial College Finite Element Program (ICFEP) (Potts and Zdravkovic, 1999, 2001) was used for all these analyses.

Geometry

Most of the results presented in this paper are for a 100 m wide building with its centre line coinciding with that of the tunnel. However, when considering the horizontal strain induced in the structure, results from analyses of a building with an eccentricity of $e=20$ m with respect to the centre lines of building and tunnel will be included. A tunnel diameter of $D=4.146$ m is modelled with a tunnel depth of either $z_0=20$ m or 34 m. These tunnel dimensions are typical for the London underground system and were used by Potts and Addenbrooke (1997) in their analyses.

Soil Properties and Initial Stresses

The soil profile consists of London clay represented by a non-linear elasto-plastic constitutive model. The model described by Jardine et al. (1986) is used to model the non-linear elastic pre-yield behaviour while the yield surface and the plastic potential are described by a Mohr-Coulomb model. The non-linear elastic model accounts for reduction of soil stiffness with strain. It uses a trigonometric expression to describe G/p' and K/p' as a function of shear strain and volumetric strain respectively in the non-linear region. G is the tangent shear modulus, K is the tangent bulk modulus and p' is the mean effective stress. It can be seen that both the shear and the bulk modulus are directly proportional to the mean effective stress. The soil parameters used for these models can be found in Appendix I.

The initial stresses in the ground are controlled by the unit weight of the soil ($\gamma=20$ kN/m^3) and by the depth of the water table (2 m). A hydrostatic pore water pressure distribution is prescribed with a zone of suction in the two metres above the water table. An earth pressure coefficient at rest of $K_0=1.5$ is applied to the whole soil strata, in contrast to the use of a K_0-reduced zone around the tunnel (Addenbrooke, 1996) in order to obtain better results for the greenfield settlement prediction. It should be noted that this latter approach was used by Potts and Addenbrooke (1997).

In the analysis presented here such a zone would not be reasonable as the building construction is necessarily simulated long before tunnel construction begins. It has been demonstrated by Addenbrooke et al. (1997) that numerical predictions of tunnelling in a high K_0 environment using reasonable soil parameters give greenfield settlement troughs which are too shallow and wide. When calculating modification factors in this study the results are related to such a greenfield trough. This has to be considered when comparing the 'weightless' results of this study with the upper bound curves from the set of analyses by Potts and Addenbrooke (1997): It will be seen that the data differ slightly due to these different initial conditions, however, these differences are small. The general principles in ground movement mechanisms which are discussed in this paper are therefore not affected by the different choice of K_0 conditions.

Modelling of the Building

The building is modelled by an elastic beam with a Young's modulus E, a second moment of area I and cross sectional area A. A building is considered to consist of a certain number of storeys. For a building with n storeys the input parameters are calculated assuming that the building consists of $n+1$ slabs with a vertical spacing of 3.4 m (*see* Fig. 3). The second moment of area for the equivalent single beam is calculated using the parallel axis theorem (Timoshenko, 1955) assuming the neutral axis to be at the mid-height of the building. Axial straining is assumed along each structure's full height to give the axial stiffness. In this study 1-, 3-, 5- and 10-storey buildings are considered. The stiffness parameters for these structures are summarized in Table 1. Greenfield conditions are modelled using a beam with a negligible stiffness and are referred to as 'flexible' cases. More details about the calculation of the elastic beam parameters are given in Appendix II (the use of an elastic beam simulating a building is a major simplification in this study. It is, however, consistent with the critical strain concept of

Table 1. Stiffness of buildings. A *n*-storey building consists of $n+1$ slabs

Building	Bending stiffness EI [kNm^2/m]	Axial stiffness EA [kN/m]
Slab	6.47×10^3	3.45×10^6
1-storey	2.00×10^7	6.90×10^6
3-storey	2.00×10^8	1.38×10^7
5-storey	6.98×10^8	2.07×10^7
10-storey	4.39×10^9	3.80×10^7

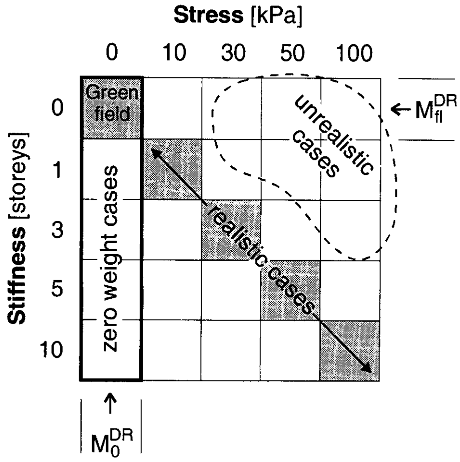

Fig. 5. Matrix of stiffness/stress combinations used in the parametric study

Burland and Wroth (1974) which uses elastic beam theory to calculate the strain within a structure). The building is assumed to be connected to the soil such that the full soil strength can be mobilised at the interface.

The building load is applied as a uniform stress of 10 kPa, 30 kPa, 50 kPa and 100 kPa to the elastic beam corresponding to a 1-, 3-, 5-, and 10-storey building respectively. In addition, zero-load cases are considered.

Combining the 5 load options with the 5 stiffness values gives 25 variations. These are represented in a 5×5 matrix in Fig. 5. The matrix contains some unrealistic cases, for instance structures with a low stiffness but loaded with a high stress. On the other hand, the leading diagonal of this matrix represents realistic cases: 10 kPa applied to a 1-storey building, 30 kPa applied to a 3-storey building etc. If basement construction were considered for a given stiffness the net loading would be reduced. This, arguably, could be represented by the cases below the leading diagonal. The stiffness-load combinations in the first column are referred to as zero-load cases (index '0'). These combinations are equivalent to the cases investigated by Potts and Addenbrooke (1997). The flexible cases can be found in the first row denoted with an index 'fl'. Combining the flexible case with the zero-load represents greenfield conditions.

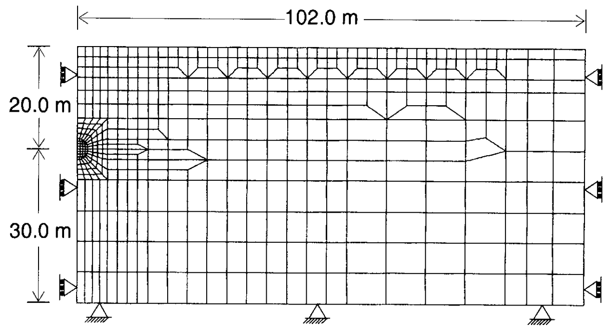

Fig. 6. Finite Element mesh for a 20 m deep tunnel with symmetrical geometry

The Sequence of the FE Analysis

Eight noded plane strain isoparametric elements are used to represent the soil. The building and the tunnel lining were modelled using three noded Mindlin beam elements. Building construction was modelled with the soil fully drained while tunnel construction was simulated with the soil behaving undrained (to achieve undrained conditions the bulk modulus of the pore water was set to be 100 times the effective bulk modulus of the soil skeleton). The mesh for a symmetrical geometry and a 20 m deep tunnel is shown in Fig. 6. As the beam representing the structure has zero thickness it cannot be seen in this figure.

The construction of the building and the ensuing tunnel excavation are simulated over several increments: A weightless beam with a stiffness representing a certain number of storeys is constructed in the first increment. Over the next increments uniform stress is applied. As this stage is modelled as being fully drained it is not necessary to simulate any consolidation period in order to reach pore water equilibrium conditions. In reality, during the consolidation time, ageing of the soil may affect the soil stiffness properties. For this reason the high initial soil stiffness to p' ratio was reset prior to tunnel excavation. This was achieved by zeroing the accumulated strains in the soil at the beginning of the first increment of tunnel excavation. As a result the initial soil stiffness before tunnel excavation depends only on the stress level p' in the soil and therefore on the applied building load.

The tunnel is then excavated over 15 increments. This is done by evaluating the stresses which act on the tunnel boundary within the soil and applying them in the reverse direction over the 15 increments. Elements within the tunnel boundary are not included in the analysis during this procedure.

The increment in which the lining is installed is chosen in order to obtain a certain volume loss V_L. The volume loss is defined as the volume (per meter length) of soil moving into the tunnel divided by the original cross-section of the tunnel ($\pi D^2/4$ per m length of tunnel). In undrained conditions it can be established by integrating the volume of the surface settlement trough. To achieve a typical value of $V_L=1.5\%$, the lining is installed on completion of the 7th excavation increment. This volume loss is detected on this particular increment when a greenfield excavation is analysed. All data for the results presented in this paper are taken from this increment. It should be noted that with different building loads the volume loss varies. For a 5-storey building and a 34 m deep tunnel the volume loss at the 7th increment of excavation reduces from $V_L = 1.50\%$ for the case with no load to $V_L = 1.40\%$ for a load of 100 kPa. The influence of the building stiffness on the volume loss is, in contrast, negligible. This study will focus on this variation of volume loss when investigating the stress state around the tunnel.

Calculation of Building Damage Parameter

To compare the results of this study with the work of Potts and Addenbrooke (1997), the deflection ratio *DR* and horizontal strain ε_h are calculated for each analysis. For calculating the deflection ratio the point of inflection has to be determined. The point of inflection separates the structure into a zone of sagging and hogging deformation as shown in Fig. 1. This point is found by calculating the rate of change of slope (i.e. the 2nd differentiation of the settlement trough) numerically in a spread sheet and locating where it changes its sign. The deflection ratio is then calculated for both sagging and hogging by dividing the maximum deflection Δ by the length L, connecting the point of inflection with the end of the structure (*see* Fig. 1). The horizontal strain ε_h is obtained directly from the ICFEP output. It is given as the maximum compressive or tensile horizontal strain of the neutral axis of the beam elements and does therefore not include any bending effects.

STRESS STATE

The construction of the building and the subsequent loading during construction changes the stress conditions in the soil. While the building stiffness changes the boundary conditions at the surface, the load affects the soil behaviour down to a depth where the tunnel will be constructed at a later stage. The effective stresses change during and subsequent to construction. The ageing process ongoing with in the soil between the end of building construction and the start of tunnel excavation might also affect the soil behaviour.

The response of the soil to the tunnel excavation depends on the stress state which also controls the soil stiffness. It will be demonstrated later how the stress state at tunnel depth controls the soil displacement while the change in soil stiffness beneath the building influences the building deformation.

These different zones of influence can be seen in Fig. 7 which shows the horizontal soil displacement in response to tunnelling plotted against depth for a vertical line at an offset of 6 m from the centre line of the building and tunnel. Different curves are presented for different loads applied by a 5-storey building. It can be seen how the building load influences the displacement behaviour near to the tunnel depth of $z_0 = 34$ m. As the load increases, the soil movement towards the tunnel reduces (a negative

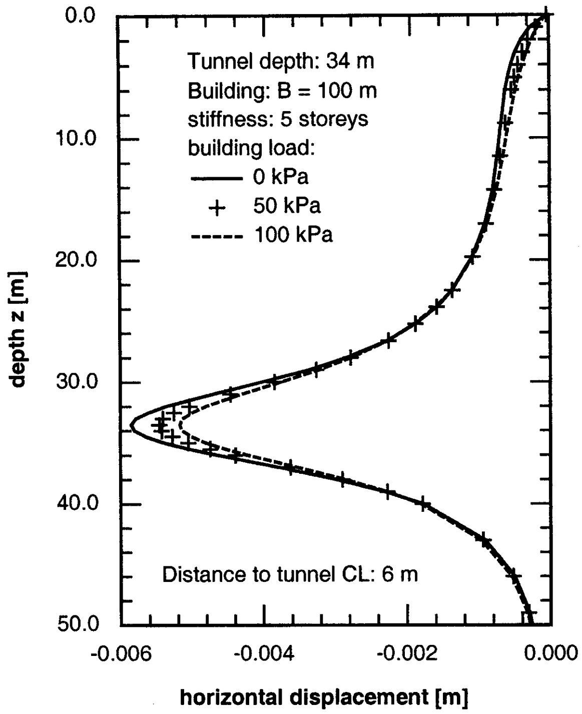

Fig. 7. Vertical profile of horizontal soil movement during tunnel construction at 6 m from centre line of tunnel

sign describes movement towards the tunnel). A similar pattern can be seen close to the building where the higher load reduces the horizontal soil displacement. At the very surface, the soil movement is restricted by the axial stiffness of the structure.

Figure 8 shows the effect of the building load on the mean effective stress p' prior to tunnel construction. The mean effective stress p' in this graph is normalized by p'_0 which is the mean effective stress of the corresponding zero-load case. The initial value of $p' = 26.16\ \mathrm{kN/m^2}$ at the surface for the zero-load case is due to the negative pore water pressure assumed above the water table.

It can be seen that the increase in stress becomes more significant towards the surface where the overburden pressure does not dominate the stress regime. This is most marked for the 100 kPa case where the stress is increased by 175% at the soil surface but only by 7% at a depth of 34 m. As the soil stiffness is modelled to be directly proportional to the mean effective stress p', the profiles in Fig. 8 therefore also indicate the increase of soil stiffness due to the application of the load. As the overburden pressure of the soil increases with depth, the effect of the building load becomes less significant. This effect can be seen in Table 2 which summarizes the stress state at 34 m depth prior to tunnel construction under a 5-storey structure. At this depth the mean effective stress p' (and the soil stiffness) increases by 7% when a load of 100 kPa is applied. The values for no building load (0 kPa) represent the initial conditions in the soil at the beginning of each analysis with a lateral stress ratio set to $K_0 = \sigma'_h / \sigma'_v = 1.5$. This ratio, however, decreases when load is applied to the structure: The ratio decreases to 1.21 when a building

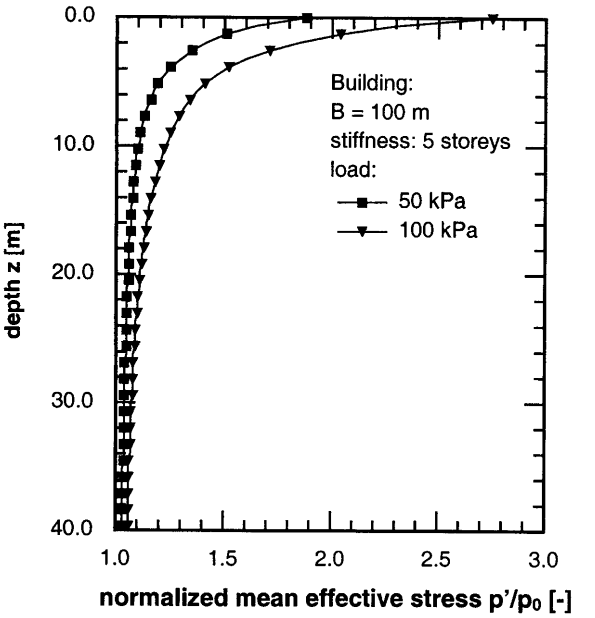

Fig. 8. Profile of normalized mean effective stress p' on centre line of building prior to tunnel construction

Table 3. Stress state scenario 1: Constant lateral stress ratio, while p' is varied

Load [kPa] (*not applied*)	0	10	30	50	100
p' [kPa]	486.9	489.7	497.2	504.0	518.7
σ'_h/σ'_v	1.50	1.50	1.50	1.50	1.50
γ_{Soil} [kN/m^3]	20.0	20.03	20.19	20.34	20.67
V_L [%]	1.50	1.48	1.46	1.45	1.42

Table 4. Stress state scenario 2: Constant p' while the lateral stress ratio is varied

Load [kPa] (*not applied*)	0	10	30	50	100
p' [kPa]	486.9	486.9	486.9	486.9	486.9
σ'_h/σ'_v	1.50	1.46	1.40	1.34	1.21
γ_{Soil} [kN/m^3]	20.0	20.18	20.55	20.92	21.82
V_L [%]	1.50	1.48	1.47	1.47	1.49

Table 2. Stress state at $z=34$ m prior to tunnel construction depending on applied building load

Load [kPa] (*applied*)	0	10	30	50	100
p' [kPa]	486.9	489.7	497.2	504.0	518.7
p'/p'_0	1.00	1.01	1.02	1.04	1.07
σ'_h/σ'_v	1.50	1.46	1.40	1.34	1.21
γ_{Soil} [kN/m^3]	20.0	20.0	20.0	20.0	20.0
V_L [%]	1.50	1.47	1.45	1.43	1.40

load of 100 kPa is imposed.

The soil behaviour in both zones, i.e. at tunnel depth and in vicinity of the structure, are investigated in the following two sections.

BEHAVIOUR AT TUNNEL DEPTH

The stress state at tunnel depth controls directly the deformation field caused by tunnel construction as it defines the loads removed from the soil during the excavation process. The soil movements around the tunnel, however, also depend on the soil stiffness which is stress level dependent. In order to separate these effects, further analyses were undertaken with no building load applied but with different soil unit weights creating the following stress scenarios at tunnel depth:

1) $\sigma'_h/\sigma'_v=1.5$ as though there were no building, p' (and soil stiffness) varying as though there were, *see* Table 3.
2) σ'_h/σ'_v varying as though there were a building, $p'=$ 487 kPa as though there were not, *see* Table 4.

The analyses were then carried out applying a 5-storey building with no load. The results of these analyses are presented as vertical profiles of horizontal displacement at a distance of 6 m from the tunnel axis. Figure 9(a) shows the displacement profile for the first stress situation (constant K_0). Each curve represents a different value of mean effective stress which is equal to the stress observed under the corresponding building load. The pattern at the level of the tunnel axis is similar to that shown in Fig. 7. As the mean effective stress increases (in Fig. 7 caused by a higher building load) the horizontal displacement reduces. The displacement in Fig. 9(a) only depends on p', in contrast to Fig. 7 where both the lateral stress ratio and the mean effective stress were varied. The increase of soil stiffness due to the increased mean effective stress p' around the tunnel explains the smaller movement and leads to smaller volume losses as shown in Table 3.

Potts and Addenbrooke (1997) showed that soil displacement is linearly related to the volume loss. Figure 9(b) shows the curves of Fig. 9(a) divided by the corresponding volume loss V_L. The fact that the curves for different load cases coincide in this plot demonstrates that the different displacement behaviour observed for different values of mean effective stress in Fig. 9(a) is simply a consequence of the different values of volume loss.

In the second stress scenario, *see* Table 4, the mean effective stress p' at tunnel axis level is constant (so the soil stiffness is constant) and only the lateral stress ratio σ'_h/σ'_v varies according to the corresponding values when the building load is applied. In Fig. 10(a), it can be seen that, again, the horizontal displacement decreases with stress states representing a higher building load. The variation in volume loss for these cases is small as shown in Table 4. When the results are divided by volume loss there are still significant differences (Fig. 10(b)). The reason for the different horizontal displacements is the

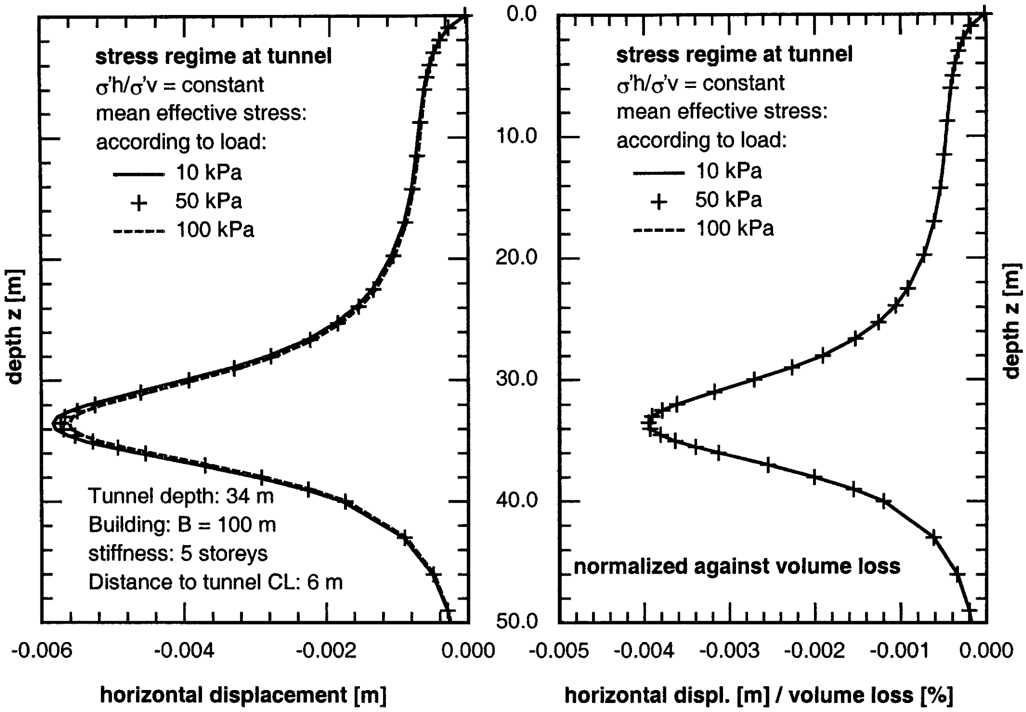

Fig. 9. (a) Vertical profile of horizontal soil movement during tunnel construction for stress scenario 1 and (b) Horizontal movement normalized against volume loss

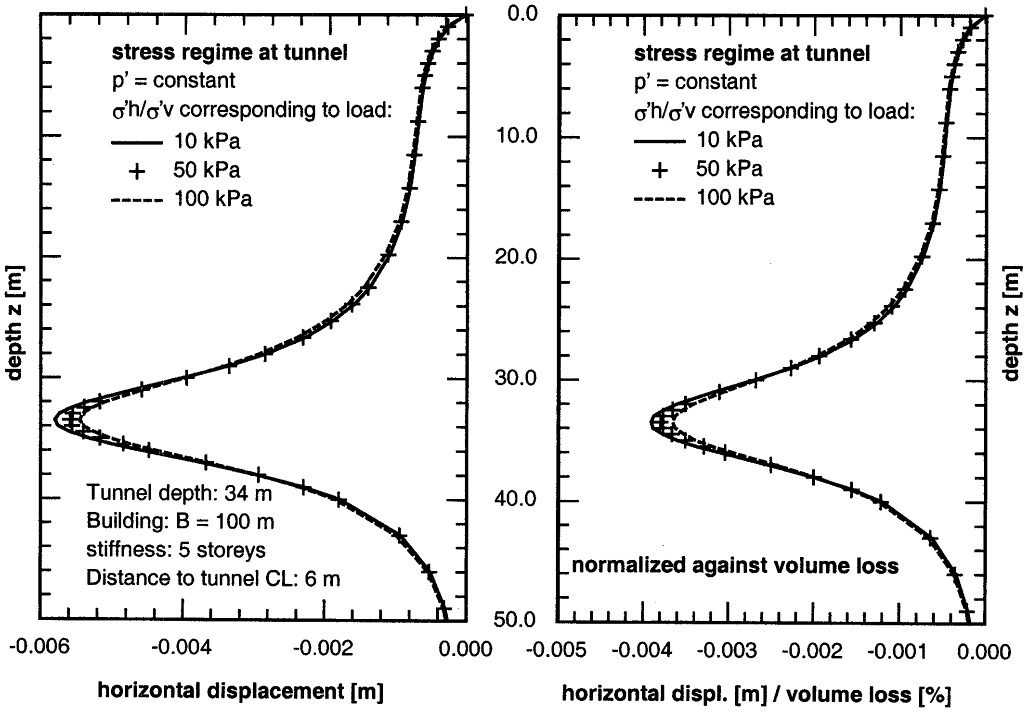

Fig. 10. (a) Vertical profile of horizontal soil movement during tunnel construction for stress scenario 2 and (b) Horizontal movement normalized against volume loss

change of deformation mode of the tunnel boundary when subjected to different σ_h'/σ_v' regimes.

Figure 7 showed that the application of building load altered the ground response to tunnelling. This is because building load changes both the mean effective stress and the σ_h'/σ_v' ratio at tunnel depth. Figures 9 and 10 have revealed that the change in mean effective stress affects the volume loss, and can be neglected when the results are adjusted to a constant volume loss. But crucially, such adjustment cannot account for the effect of different lateral stress ratios.

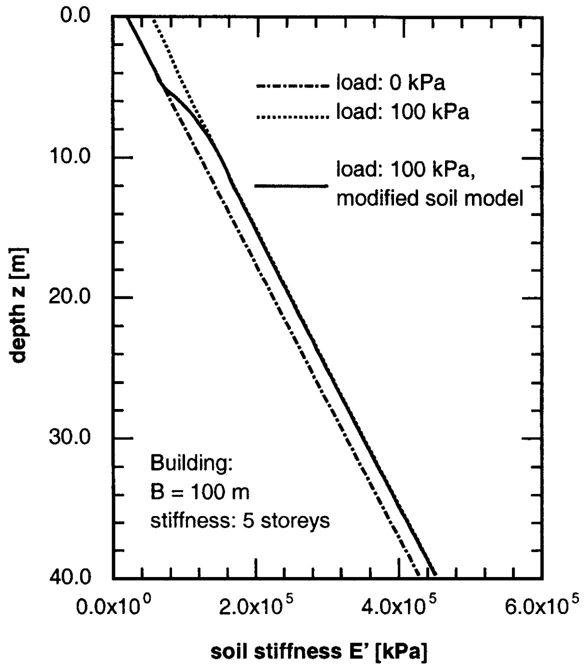

Fig. 11. Soil stiffness profile on centre line of building prior to tunnel construction

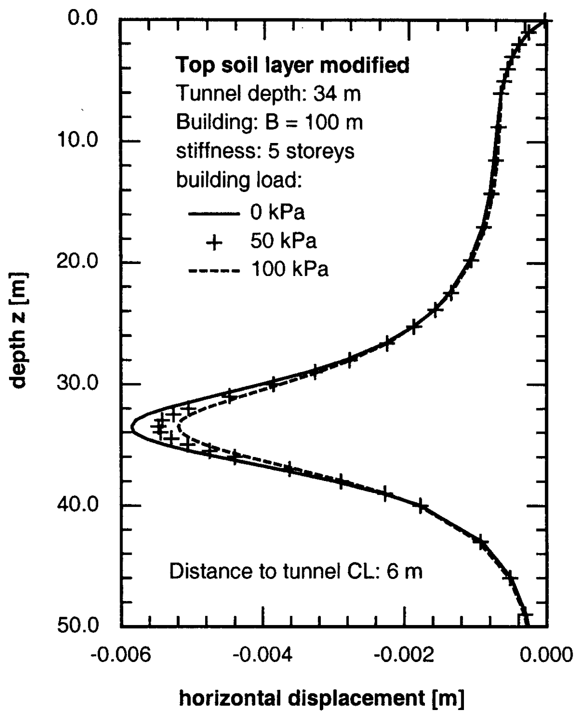

Fig. 12. Vertical profile of horizontal soil movement during tunnel construction for modified soil model used in top 6 m soil layer

BEHAVIOUR UNDER THE FOUNDATION

Figure 7 shows that the tunnelling induced horizontal ground movement near the surface is affected by the applied building load. Prior to tunnel construction all strains in the soil are set to zero. Consequently, the initial soil stiffness immediately prior to tunnel construction only depends on the level of mean effective stress p'. The dotted lines in Fig. 11 show this situation. For the zero-load case, the stiffness increases linearly with depth. The soil stiffness for the 100 kPa load is higher due to the increased stress level.

To investigate how the soil movement in response to tunnelling is influenced by the soil stiffness in close proximity to the foundation, further analyses were undertaken using a modified soil model for the uppermost 6 m of soil. A depth of 6 m was chosen as it corresponds to the depth where the maximum variation of horizontal ground movement with load was found (shown in Fig. 7). The soil stiffness parameters in this layer are chosen to increase linearly with depth to match the stiffness distribution given by the zero-load case. The analyses then undertaken for a 5-storey building comprises different load cases of 0 kPa, 50 kPa and 100 kPa. For the 100 kPa case, the stiffness profile prior to tunnel construction is shown by the solid line in Fig. 11.

When using the non-linear elastic model in the upper 6 m, the soil stiffness reduces with increasing strain level during tunnel excavation. This effect is reproduced in the modified soil layer by changing the elastic properties during each excavation increment. The soil stiffness in that zone therefore represents, at each stage of the excavation, the soil stiffness found in a zero-load analysis in the corresponding excavation increment. By this modification, the soil stiffness in the uppermost 6 m is not influenced by the building load.

Figure 12 presents the results of the analyses plotted as a profile of horizontal displacement with depth for a distance from the tunnel centre line of $x=6$ m. There is a uniform horizontal displacement for all load cases in the top 6 m of soil which coincides with the zero-load case (without modified soil layer) shown in Fig. 7. Below this depth the displacement follows the pattern observed in Fig. 7. These analyses show that it is the soil stiffness in the zone beneath the foundation which controls the horizontal displacements in this region, and not the change in σ'_h/σ'_v ratio.

PARAMETRIC STUDY: DEFLECTION RATIO

For the 100 m building without eccentricity, all stiffness-load combinations shown in Fig. 5 were analysed in order to obtain an overall picture of the influence of building load on the deflection ratio.

For all 50 cases, the deflection ratios DR_{hog} for hogging and DR_{sag} for sagging were determined. Dividing these values by the corresponding greenfield values (given in Table 5) gives the modification factors M^{DR}. The results of each stiffness are then normalized against the corresponding zero-load modification factor M_0^{DR} (*see* Fig. 5). The data are presented in graphs showing (M^{DR}/M_0^{DR}) versus building load. Figures 13 and 14 show these plots for hogging and sagging respectively. In order to obtain these results, the deflection ratio is adjusted in each case to a common volume loss of $V_L=1.5\%$.

For hogging, Fig. 13 shows for each stiffness (given by

Table 5. Deflection ratio and horizontal strain for greenfield conditions

Geometry: $e=0$ m, $B=100$ m		
$z_0=20$ m	$DR_{hog}=2.16\times10^{-5}$	$DR_{sag}=5.75\times10^{-5}$
$z_0=34$ m	$DR_{hog}=6.38\times10^{-6}$	$DR_{sag}=1.98\times10^{-5}$
Geometry: $e=20$ m, $B=100$ m		
$z_0=20$ m	$\varepsilon_{ht}=7.66\times10^{-5}$	$\varepsilon_{hc}=-3.54\times10^{-4}$
$z_0=34$ m	$\varepsilon_{ht}=3.01\times10^{-5}$	$\varepsilon_{hc}=-1.31\times10^{-4}$

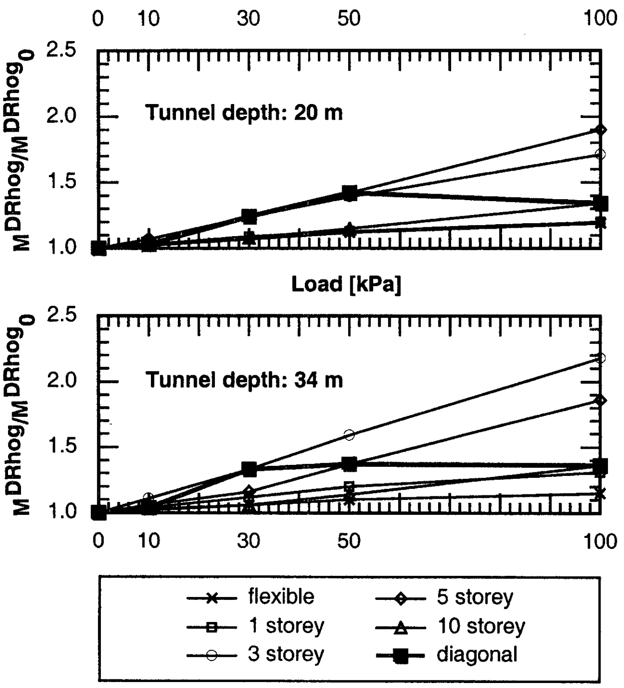

Fig. 13. Change of hogging modification factor M^{DR}_{hog} with applied stress. M^{DR}_{hog} normalized against corresponding zero-load case

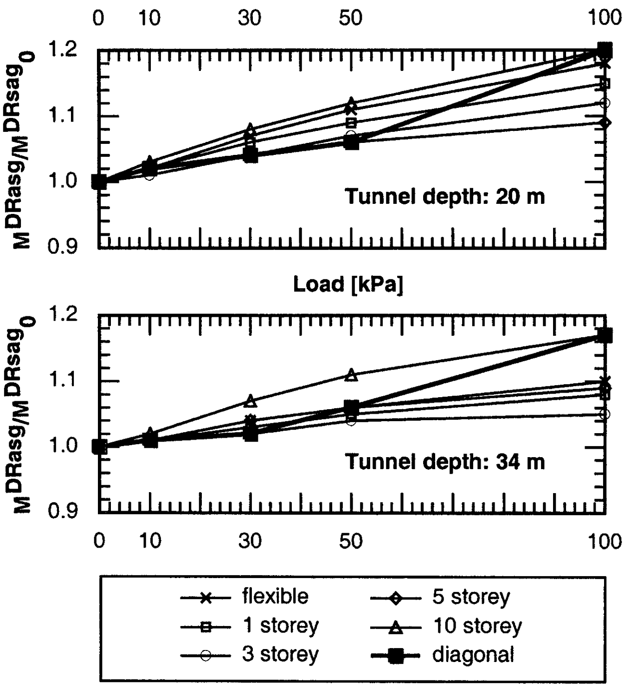

Fig. 14. Change of sagging modification factor M^{DR}_{sag} with applied stress. M^{DR}_{sag} normalized against corresponding zero-load case

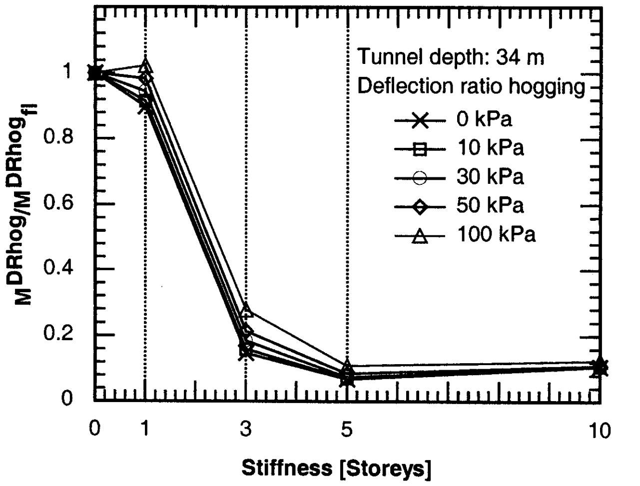

Fig. 15. Change of modification factor M^{DR}_{hog} with stiffness. M^{DR}_{hog} normalized against corresponding flexible case (0 storey)

the number of storeys) a steady increase in the modification factor M^{DR}_{hog} with increasing building load. This effect is small for structures with a low stiffness (0 and 1 storey) and a high stiffness (10 storeys) but is more significant for the 3 and 5 storey cases. It is appropriate to focus on the realistic cases (i.e. those on the leading diagonal in Fig. 5). The data for these cases are marked with a thick line and black squares. The biggest increase is 42% for the 5-storey building and a tunnel depth $z_0=20$ m. For the sagging case shown in Fig. 14, the change of modification factor M^{DR}_{sag} is smaller than for hogging (note the different scale between Figs. 13 and 14). The maximal increase is 20% for the 10-storey building and a 20 m deep tunnel. Although the increases for both cases seem to be significant, it must be noted that the deflection ratio decreases rapidly as building stiffness increases. Figure 15 gives a clear picture of this as the modification factor for each magnitude of applied load is normalized against the corresponding result for the flexible structure, M^{DR}_{fl}. The data for hogging above the 34 m deep tunnel are plotted against the structure's stiffness. The data lie in a very narrow range and show a significant decrease of between 70 and 85% as the stiffness increases from 1 storey up to 3 storeys. For higher stiffness values, the results are stable and the deflection ratio is about 10% of the corresponding value for the flexible structure. This clearly shows that building stiffness dominates the problem, not building weight.

This is further illustrated in Fig. 16 where the modification factors for hogging and sagging are plotted against the relative bending stiffness ρ^*. For all stiffness values, the results for the zero-load (square symbols) and for the 'realistic' case (on the leading diagonal, triangle symbols) lie almost on top of each other. Even the 42% increase of modification factor mentioned above is small when plotted in this context. The increase is from $M^{DR}_{hog}=0.053$ for the zero-weight case to $M^{DR}_{hog}=0.076$ for the case considering self weight. Following the design approach by Potts and Addenbrooke (1997), this means for engineering practice that M^{DR}_{hog} for a 5-storey building affected by tunnelling induced ground subsidence is only 0.076 times the hogging ratio for the corresponding greenfield situation.

The corresponding design curves by Potts and Addenbrooke (1997) which were an upper bound to their design data, are shown for comparison and they are an upper bound to the data from these analyses, too.

The soil stiffness E_s used for describing the relative bending stiffness Eq. (1) is taken at a depth half way between the tunnel axis and the ground surface. In the analyses of Potts and Addenbrooke (1997) this value is only dependent on the depth of the tunnel. In the data presented in Fig. 16, the increase in E_s due to the increased effective stress p' under the building load is taken into account. The difference in relative stiffness for each data couple in this graph is, however, small.

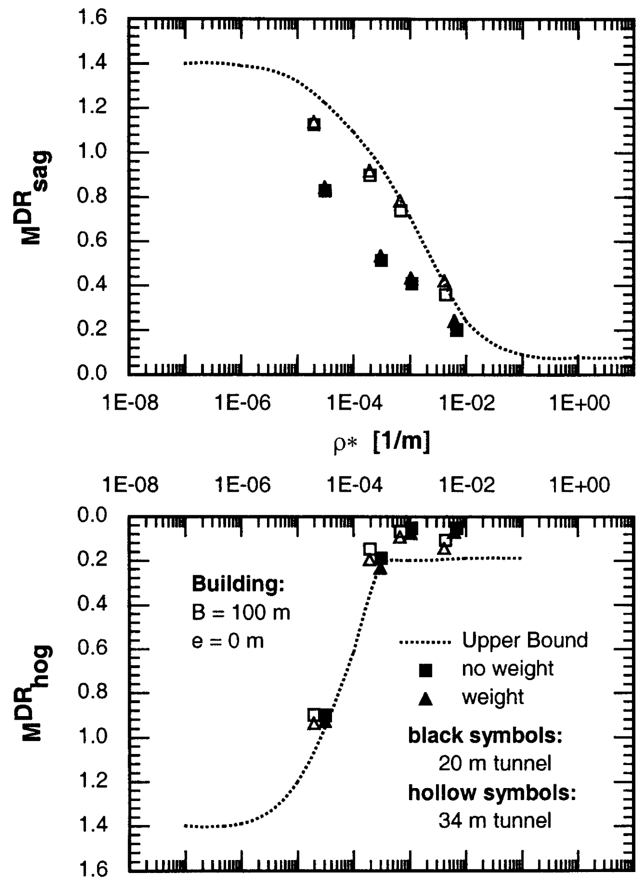

Fig. 16. Modification factors M^{DR} together with the design curves by Potts and Addenbrooke (1997)

PARAMETRIC STUDY: HORIZONTAL STRAIN

The second building damage parameter adopted in this study is the horizontal strain ε_h. It was found that hardly any tensile strain occurs in a 100 m wide building with no eccentricity. Therefore, additional analyses were performed in which the building had an eccentricity of $e=20$ m with respect to the centre line of the tunnel. Figure 17(a) shows the strain distribution over the length of the 5-storey building. The results for the zero-load, the 50 kPa and the 100 kPa case are presented. The increase (in terms of absolute value) in both compressive (negative sign) and tensile (positive sign) strain can be seen. In a previous section it was demonstrated how the soil stiffness in close proximity to the building controls the horizontal displacement of the soil in this region. A set of analyses using the modified soil model for the uppermost

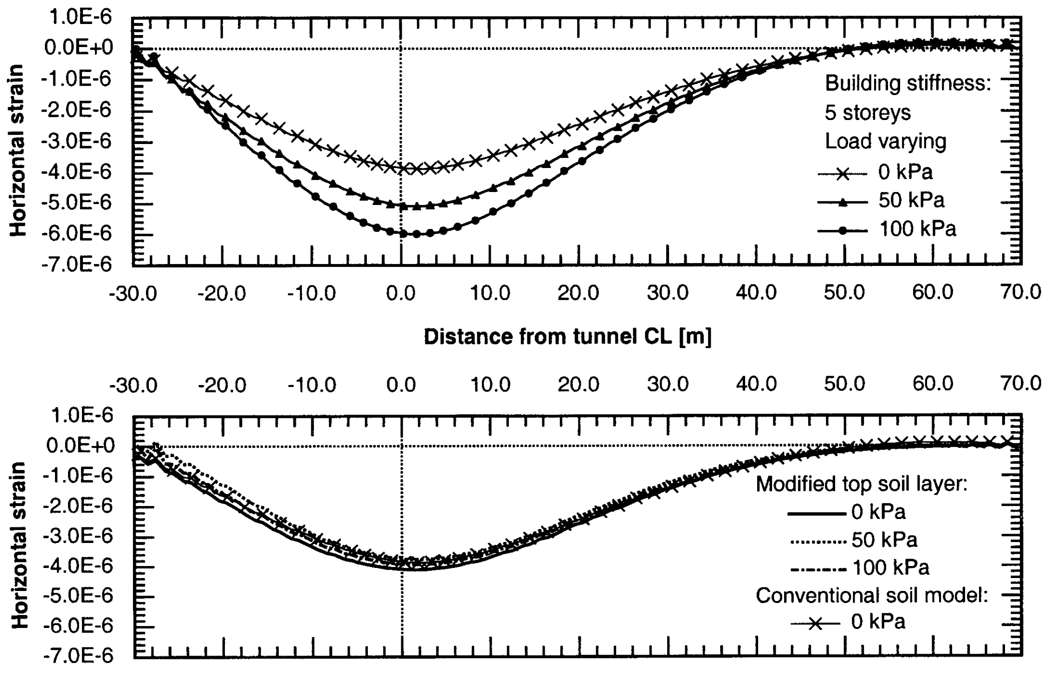

Fig. 17. Horizontal strain distribution in structure ($B=100$ m, $e=20$ m, $z_0=34$ m)

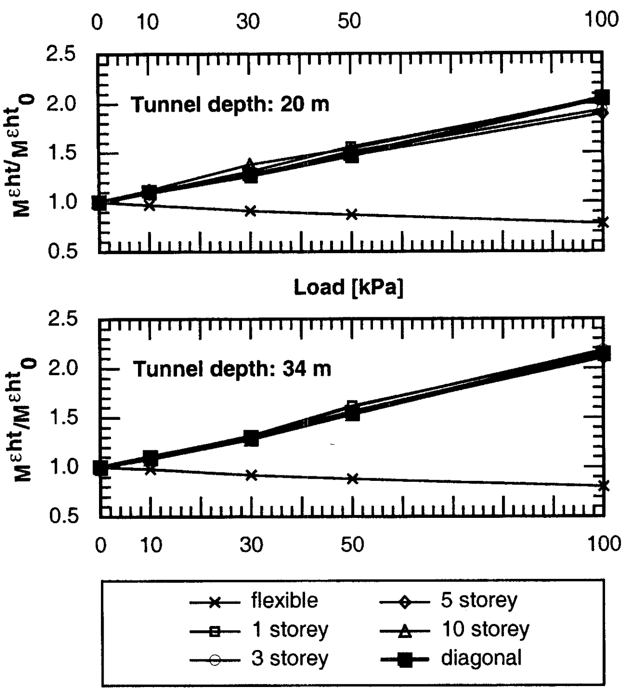

Fig. 18. Change of tensile strain modification factor $M^{\varepsilon}_{\mathrm{ht}}$ with applied stress. $M^{\varepsilon}_{\mathrm{ht}}$ normalized against corresponding zero-load case

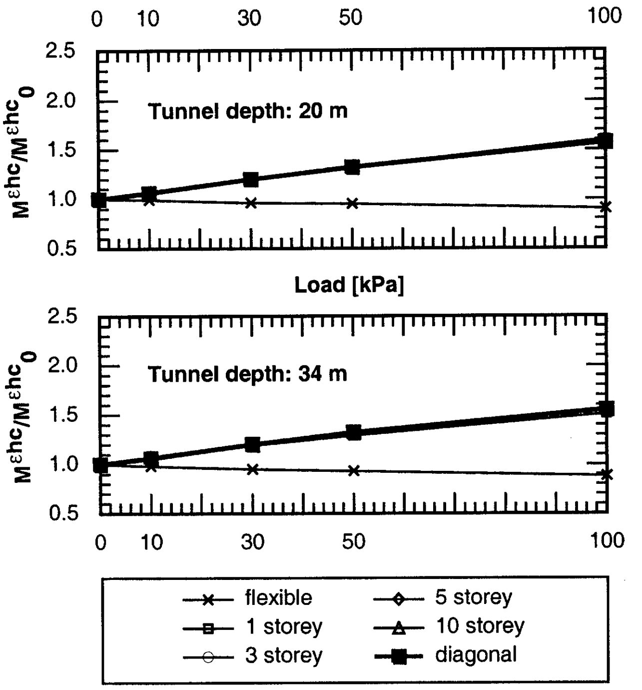

Fig. 19. Change of compressive strain modification factor $M^{\varepsilon}_{\mathrm{hc}}$ with applied stress. $M^{\varepsilon}_{\mathrm{hc}}$ normalized against corresponding zero-load case

6 m of soil (*see* Fig. 11) was undertaken with the eccentric building geometry. Figure 17(b) shows the strain distribution from these analyses. The lines for different load cases lie close together and coincide well with the zero-load case using the conventional soil model. This result reveals how the stiffness in the uppermost soil controls the strain development in the structure caused by tunnelling: On the one hand, the higher soil stiffness reduces the horizontal soil movement whereas, on the other hand, it means the soil is more able to transfer this movement to the structure. The net result is an increase in horizontal strain.

This effect can be observed for all stiffness-load combinations. Figures 18 and 19 show the development of horizontal strain when the building load is increased. The plots are of a similar format to those shown in Figs. 13 and 14 with the modification factors $M^{\varepsilon}_{\mathrm{h}}$ for each load case normalized against the corresponding zero-load case. For the flexible structure, the modification factors reduce slightly with increasing load. This is due to the absence of any stiff structure restraining the horizontal movement of the soil. Hence, the reduction in modification factors is caused by the reduction in horizontal soil movement with increasing soil stiffness. If, however, a stiff structure is included into the analyses this picture changes: for the 1-, 3-, 5- and 10-storey buildings the horizontal strain (both compression and tension) in the structure increases steadily with building load. For both tensile and compressive strain the behaviour for each tunnel depth is very similar. The tensile strain is increased by approximately 100% when a load of 100 kPa is applied compared to the zero-load case. For the compressive strain this increase is smaller giving a compressive strain that is 50% greater than in the corresponding zero-load case when 100 kPa are applied.

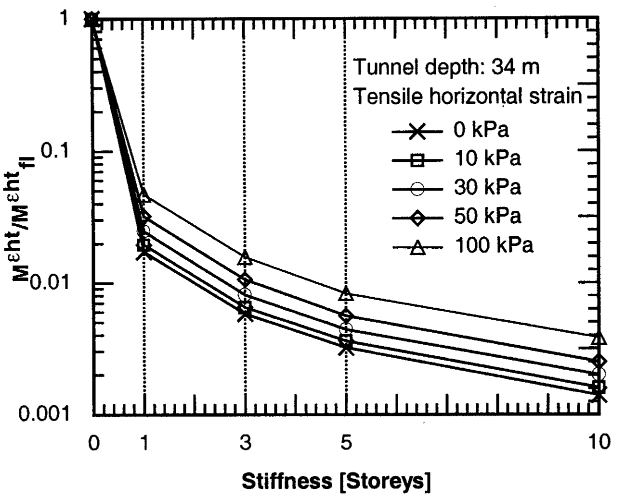

Fig. 20. Change of tensile strain modification factor $M^{\varepsilon}_{\mathrm{ht}}$ with stiffness. $M^{\varepsilon}_{\mathrm{ht}}$ normalized against corresponding flexible case (0 storey)

These graphs, however, give no indication about the absolute magnitude of horizontal strain developed in the structure. Figure 20 shows that the strain drops significantly when normalizing the modification factors against the corresponding flexible case (note that in contrast to Fig. 15 this graph has a logarithmic scale on the ordinate): As an example, the data for tension and for the 34 m deep tunnel are given, showing a significant reduction to values between 0.017 and 0.05 for the 1-storey stiffness compared to the flexible case. Combining these results with the curves in Fig. 18 reveals that

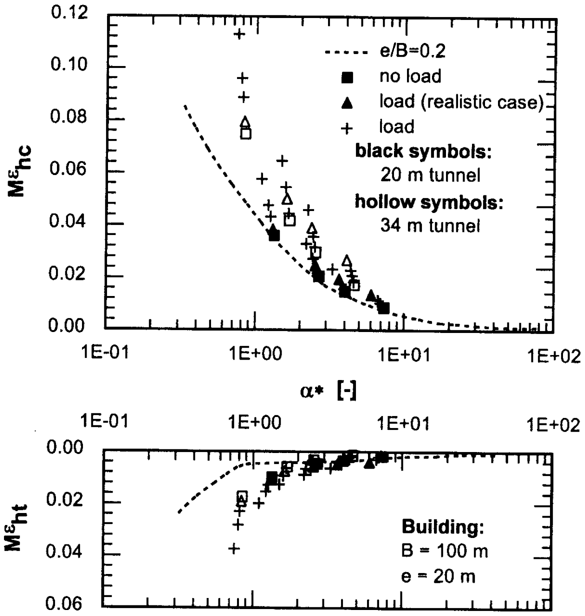

Fig. 21. Strain modification factors $M^{\varepsilon h}$ together with the design curves by Potts and Addenbrooke (1997)

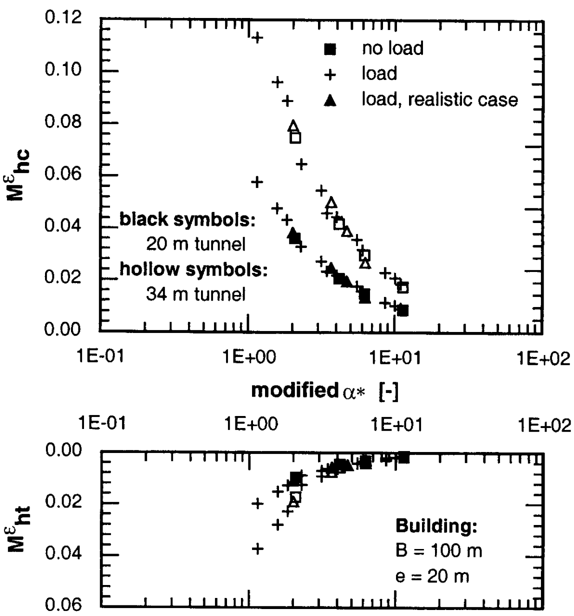

Fig. 22. Strain modification factors $M^{\varepsilon h}$ versus a modified relative axial stiffness taking into account the change of soil stiffness beneath the foundation

although there is a clear trend of increasing modification factor with load, the modification factors themselves remain at a very low level. This becomes clear when plotting the modification factors against the relative axial stiffness α^*. Figure 21 includes all the load cases. The zero-load cases are marked with square symbols while the 'realistic' cases are represented by triangle symbols. All other cases are shown with a cross symbol. Because of the small scale chosen in this graph, the increase in modification factors for all cases when load is considered can clearly be seen. The realistic cases, however, remain close to the corresponding zero-load square symbols.

Figure 21 also shows the design curves by Potts and Addenbrooke (1997). It can be seen that some 'weightless' results lie above the curves for an eccentricity of $e/B=0.2$. This is due to the changed initial conditions (i.e. no zone of reduced K_0) used in these analyses. It is therefore not possible to compare the results of the present work directly with the study of Potts and Addenbrooke (1997). However, as the difference between the current data and their upper bound curves remains small it is still possible to use their design approach.

This graph reveals that the modification factors remain small with a maximum value of $M^{\varepsilon}_{hc}=0.08$ for the 1-storey building under a load of 10 kPa, $z_0=34$ m. According to the design approach by Potts and Addenbrooke (1997) this means that the horizontal compressive strain in this type of structure is only 0.08 times the compressive strain found in the corresponding greenfield situation. These greenfield values are given in Table 5. For the tensile strain (which is more critical in respect to building damage) the modification factor is even smaller: $M^{\varepsilon}_{ht}=0.02$ for the 1-storey structure mentioned above.

For calculating the relative axial stiffness α^*, the soil stiffness E_s considered in Eq. (1) is taken at half tunnel depth. For the results shown in Fig. 21, the increase of E_s due to the increase of p' at this depth is taken into account. It can be seen that the difference in relative axial stiffness for each range of load cases is very small. Previously, it was shown that it is the soil stiffness in a zone immediately beneath the building which controls the horizontal strain behaviour in the building. It is therefore straightforward to include this soil stiffness into the relative axial stiffness α^*. For this particular geometry, the best curve fit can be achieved when taking the soil stiffness from a depth of $z=5.8$ m. Figure 22 shows the strain modification factors for all stiffness-load combination plotted against the modified relative axial stiffness incorporating the soil stiffness at $z=5.8$ m. It can be seen that for each tunnel depth the data points follow a uniform line with a very small scatter.

Although choosing the soil stiffness at $z_0=5.8$ m seems to be an arbitrary choice, the result demonstrates the significant influence of the soil stiffness below the structure's foundation. Figure 22 shows different patterns for each tunnel depth. This is because the tunnel depth z_0 is not included anymore in the modified relative stiffness α^* while it was incorporated into the original formulation when the soil stiffness was taken from half tunnel depth.

In an engineering context the increase of modification factors for realistic stiffness-load combinations remains very small. These results lie very close to the design curves provided by Potts and Addenbrooke (1997). The scatter shown in Fig. 21 is small compared to the potential error associated with the estimation of the structure's stiffness.

CONCLUSIONS

This paper shows the influence of the weight of a structure on its deformation behaviour caused by tunnelling induced ground subsidence. Using the Finite Element

Table 6. Material parameters used in non-linear elastic model

A	B	C [%]	α	γ	E_{dmin} [%]	E_{dmax} [%]	G_{min} [kPa]
373.3	338.7	1.0E-4	1.335	0.617	8.66025×10^{-4}	0.69282	2333.3
R	S	T [%]	δ	μ	ε_{vmin} [%]	ε_{vmax} [%]	K_{min} [kPa]
549.0	506.0	1.0E-3	2.069	0.420	5.0×10^{-3}	0.15	3000.0

Method, loads of up to 100 kPa were applied to structures with a bending stiffness ranging from 2.00×10^7 kNm^2/m to 4.39×10^9 kNm^2/m and an axial stiffness between 6.9×10^6 kN/m and 3.80×10^7 kN/m representing 1 to 10 storey buildings. The soil profile consisted of London clay.

By varying the material properties of the soil profile the mechanisms which control this soil-structure interaction problem were investigated. It was found that the load of the building alters the deformation behaviour of the soil in two distinct zones: at tunnel depth and in close proximity to the foundation of the building.

At tunnel depth, the effect of increasing mean effective stress p' has been uncoupled from the change in lateral stress ratio σ_h'/σ_v' and the consequences of both were analysed separately. It was found that the increase in p' affects directly the volume loss V_L. Dividing the soil displacement by volume loss leads to a uniform soil movement for different levels of mean effective stress while σ_h'/σ_v' is kept constant. The lateral stress ratio σ_h'/σ_v' in contrast influences the deformation field of the soil which consequently affects any structure above the tunnel. This demonstrates the complex character of the interaction problem: the load of the building changes the stress regime which influences the deformation mode of the soil around the tunnel which then affects the response of the building to the tunnelling induced subsidence.

The increase in soil stiffness in close proximity to the structure has been found to influence the building response significantly. It has been shown that the development of horizontal strain in the structure can be directly related to the soil stiffness beneath the structure.

The influence of building load on the deflection ratio and on horizontal strain has been investigated with a parametric study involving 50 nonlinear plane strain FE analyses for two different building geometries. It has been shown that, in general, the modification factors increase with increasing load. This effect is, however, small compared to the decrease of deflection ratio and horizontal strain with increasing building stiffness. Since the latter effect dominates, the graphs plotting modification factor against relative stiffness show little change when realistic building weight scenarios are included into the analyses. The results therefore lie close to the upperbound curves provided by Potts and Addenbrooke (1997) and provide further confidence in the use of these curves for practical design.

ACKNOWLEDGEMENT

This work is part of a research project funded by the Engineering and Physical Sciences Research Council (EPSRC) with industrial collaboration with the Construction Industry and Research Information Association (CIRIA), the Geotechnical Consulting Group (GCG) and London Underground Limited (LUL).

REFERENCES

1) Addenbrooke, T. I. (1996): Numerical analysis of tunnelling in stiff clay, *PhD thesis*, Imperial College, University of London.
2) Addenbrooke, T. I., Potts, D. M. and Puzrin, A. M. (1997): The influence of pre-failure soil stiffness on the numerical analysis of tunnel construction, *Géotechnique*, **47** (3), 693–712.
3) Boscardin, M. D. and Cording, E. J. (1989): Building response to excavation induced settlement, *J. of Geotech. Engrg.*, ASCE, **115** (1), 1-21.
4) Burland, J. B. and Wroth, C. P. (1974): Settlement of buildings and associated damage, *BGS Conf. 'Settlement of Structures'*, Cambridge, 611–651.
5) Burland, J. B. (1995): Assessment of risk of damage to buildings due to tunnelling and excavatioins, *1st Int. Conf. on Earthquake Geotech. Engrg.*, IS-Tokyo '95.
6) Jardine, R. J., Potts, D. M., Fourie, A. B. and Burland, J. B. (1986): Studies of the influence of non linear stress-strain characteristics in soil-structure interaction, *Géotechnique*, **36** (3), 377–396.
7) O'Reilly, M. P. and New, B. M. (1982): Settlements above tunnels in the United Kingdom-their magnitude and prediction, *Tunnelling '82*, The Inst. of Mining and Metallurgy, 173–181.
8) Potts, D. M. and Addenbrooke, T. I. (1997): A structure's influence on tunnelling-induced ground movements, *Proc. Inst. of Civil Engineers, Geotech. Engrg.*, **125**, 109–125.
9) Potts, D. M. and Zdravkovic, L. (1999): *Finite Eelement Analysis in Geotechnical Engineering: Theory*, Thomas Telford, London.
10) Potts, D. M. and Zdravkovic, L. (2001): *Finite Element Analysis in Geotechnical Engineering: Application*, Thomas Telford, London.
11) Timoshenko, S. (1955): *Strength of Materials*, 3rd ed., D. Van Nostrand Company, Inc., New York.

APPENDIX I: SOIL MODEL

The nonlinear elastic model (Jardine et al., 1986) describes the secant soil stiffness depending on the strain level using a trigonometric expression. To use this model in a finite element analysis, the secant expressions are differentiated and then normalized against mean effective stress giving the following tangent values (Potts and Zdravkovic, 1999):

$$\frac{G}{p'}=A+B\cos(\alpha X^{\gamma})-\frac{B\alpha\gamma X^{\gamma-1}}{2.303}\sin(\alpha X^{\gamma})$$

$$\text{with}\quad X=\log_{10}\left(\frac{E_d}{\sqrt{3}C}\right) \tag{A1}$$

$$\frac{K}{p'}=R+S\cos(\delta Y^{\mu})-\frac{S\delta\mu Y^{\mu-1}}{2.303}\sin(\delta Y^{\mu})$$

$$\text{with}\quad Y=\log_{10}\left(\frac{|\varepsilon_v|}{T}\right) \tag{A2}$$

where G and K are the shear modulus and bulk modulus respectively, p' is the mean effective stress, E_d the deviatoric strain invariant and ε_v is the volumetric strain. A, B, C, R, S, T, δ, α, γ, μ are constants which are listed in Table 6. E_{dmax}, E_{dmin}, ε_{vmax}, ε_{vmin} define strain limits above or below which the stiffness only varies with p' and not with strain. Minimum values of shear and bulk moduli are given by G_{min} and K_{min} respectively.

In addition, a Mohr-Coulomb model is employed in this study. The strength parameters are $c'=5.0$ kPa, $\phi'=25°$ and the angle of dilation $\psi=12.5°$.

APPENDIX II: EQUIVALENT BEAM STIFFNESS VALUES

A building with n storeys consists of $n+1$ slabs with a vertical spacing of 3.4 m (*see* Fig. 3). Each slab has the following plane strain properties:

Young's modulus:	$E_C=23.0E+6$ kN/m^2
Area:	$A_{slab}=0.150$ m^2/m
Second moment of area:	$I_{slab}=2.8125E-4$ m^4/m

The axial and bending stiffness of the structure was then calculated as:

$$(E_CA)_{struct}=(n+1)(E_CA)_{slab} \tag{A3}$$

$$(E_CI)_{struct}=E_C\sum_{1}^{(n+1)}(I_{slab}+A_{slab}H_n^2) \tag{A4}$$

where H_n is the vertical distance between the structure's and the slab's neutral axis. These values are then adjusted for plane strain conditions taking into account that the out-of-plane dimension is unity.